

Cite this: *Lab Chip*, 2012, 12, 2533–2539

www.rsc.org/loc

PAPER

In vitro and *in vivo* testing of glucose-responsive insulin-delivery microdevices in diabetic rats†

Michael K. L. Chu, Jian Chen, Claudia R. Gordijo, Simon Chiang, Alexander Ivovic, Khajag Koulajian, Adria Giacca,* Xiao Yu Wu* and Yu Sun*

Received 8th February 2012, Accepted 30th March 2012

DOI: 10.1039/c2lc40139h

We have developed glucose-responsive implantable microdevices for closed-loop delivery of insulin and conducted *in vivo* testing of these devices in diabetic rats. The microdevices consist of an albumin-based bioinorganic membrane that utilizes glucose oxidase (GOx), catalase (CAT) and manganese dioxide (MnO₂) nanoparticles to convert a change in the environmental glucose level to a pH stimulus, which regulates the volume of pH-sensitive hydrogel nanoparticles and thereby the permeability of the membrane. The membrane is integrated with microfabricated PDMS (polydimethylsiloxane) structures to form compact, stand-alone microdevices, which do not require tethering wires or tubes. During *in vitro* testing, the microdevices showed glucose-responsive insulin release over multiple cycles at clinically relevant glucose concentrations. *In vivo*, the microdevices were able to counter hyperglycemia in diabetic rats over a one-week period. The *in vitro* and *in vivo* testing results demonstrated the efficacy of closed-loop biosensing and rapid response of the ‘smart’ insulin delivery devices.

Introduction

The global effect of diabetes has been an issue that is increasingly weighing on our population. With around 285 million people affected in 2010, the number of diabetic patients is expected to drastically increase to 440 million by 2030.¹ Diabetes is marked by the destruction of islet β -cells and the inability to produce endogenous insulin, known as Type 1 diabetes, or by the development of insulin resistance and inability of the pancreas to provide adequate insulin, known as Type 2 diabetes.^{2,3} In all diabetic patients, the body is unable to control blood glucose levels, leading to a state of hyperglycemia, a precursor for further complications, such as micro/macrovacular, renal and neural damage. The necessary treatment of diabetes complications is an increasing financial burden.^{1–3}

Insulin replacement therapy is the current standard treatment for all Type 1 diabetic patients and more than one third of Type 2 diabetic patients. Directly providing exogenous insulin to lower blood glucose is required to maintain normoglycemia for these patients and is often necessary for survival.⁴ Although effective in short periods, insulin therapy cannot reproduce normal physiological insulin secretion patterns. Even when using combinations of short and long-acting insulin types, complica-

tions can arise when insulin dosage amount and timing are not precise, leading to intermittent periods of hypoglycemia due to an excess of insulin and chronic complications from periods of hyperglycemia due to lack of insulin.

Ideally, insulin therapy should provide the proper amounts of insulin in response to blood glucose concentration. Current attempts towards this goal involve the use of continuous insulin delivery *via* pumps.^{5–7} With a needle inserted in the abdominal fat, insulin is delivered subcutaneously from an insulin reservoir, providing a constant basal release of insulin, more closely mimicking the physiological insulin profile than subcutaneous injections.^{5–9} However, this treatment approach still requires regular glucose monitoring, that is, it is an open-loop approach. Combination of insulin pumps with real-time glucose sensors have been investigated for closed-loop insulin delivery by collecting blood glucose data and converting it into a release profile for responsive insulin delivery. Compared with standard pumps, the pump and sensor combination resulted in shorter durations of hypoglycemia. However, there were no significant differences in hemoglobin A1c, a measurement of long-term glycemic index.^{6,10,11}

Another glucose-responsive closed-loop insulin delivery option is the use of glucose-responsive hydrogel-based insulin delivery systems. The systems require the synergy of a real-time glucose sensor and a responsive insulin release element. Glucose oxidase has been successfully used as a glucose sensing component^{12–27} in combination with pH-responsive materials, such as films^{18–22} or hydrogel particles.^{13,14,23–27,38} The enzymatic oxidation of glucose into gluconic acid is harnessed to

Mechanical and Industrial Engineering, University of Toronto, Toronto, Ontario, Canada. E-mail: adria.giacca@utoronto.ca; xywu@phm.utoronto.ca; yu.sun@utoronto.ca

† Electronic supplementary information (ESI) available. See DOI: 10.1039/c2lc40139h

produce an acidic 'trigger' for a pH-responsive delivery system. The pH signal is utilized to modulate shrinking/swelling response^{24–27} or disintegration^{28,29} of pH-responsive hydrogels, releasing loaded insulin. The *in vivo* application of insulin-loaded hydrogel systems is limited by slow response times, clinically irrelevant glucose-responsive range, low insulin loading capacity, bioavailability, stability and non-cyclic release profiles.^{25,26,30,31}

To overcome the limitations of hydrogel systems, Yam and Wu designed hydrogel nanoparticle-containing composite membrane systems for stimulus-responsive drug delivery.^{31,32} Utilizing environment-sensitive hydrogels as physical 'nanovalves', drug delivery across the membrane is modulated by shrinking or swelling of embedded responsive nanoparticles. The nano-size allows for rapid response, within seconds, while the hydrogel polymer structure maintains three-dimensional geometry and repeatable volumetric responses. Typical hydrogel nanoparticles used in the composite membranes are comprised of crosslinked copolymers, specifically poly(*N*-isopropylacrylamide) (PNIPAM) and poly(methacrylic acid) (PMAA).³³ PMAA acts as a pH-sensor that changes ionization degree according to pH, affecting nanoparticle hydration and volume. At pH levels above pK_a , the MAA groups are ionized and the charged carboxyl groups generate repulsive forces, causing the nano-hydrogel to swell. At low pH levels, the MAA groups take the un-ionized form, causing collapse of the nano-hydrogel particles. pH-responsive membranes with embedded PNIPAM–MAA nano-hydrogels have been previously studied for pH-responsive protein/peptide drug delivery^{14,21,31,32,34,35} and incorporated into a microdevice system that provided a 2-fold increase in vitamin B₁₂ release when environmental pH drops from neutral to acidic pH.³⁶

A new generation of glucose-responsive composite membrane systems was devised by Gordijo *et al.* to address the problem of oxygen-limited glucose sensing encountered by glucose oxidase-based biosensors.²¹ Utilizing the capability of MnO₂ nanoparticles to fully recover oxygen consumed by glucose oxidation, an albumin-based bioinorganic membrane system was developed with a glucose sensing component that possesses a self-renewable oxygen supply.²¹ The bioinorganic composite membrane was integrated with an insulin reservoir to form an implantable tube-shaped microdevice made of biocompatible silicone. The device, when implanted, reduced hyperglycemia in streptozotocin (STZ) induced-diabetic rats for up to 5 days.²²

The previous tube-shaped microdevices, although proven effective in lowering hyperglycemia, exhibited certain technical restraints. Due to small surface areas for permeation limited by the construction method, the implantation of a number of these devices (*vs.* a single device) was required to achieve normoglycemic state in STZ-diabetic rats. In addition, the smaller reservoir volume limited the total amount of insulin that can be stored. Hence, in this work we intended to develop a microdevice with larger permeation surface area and reservoir volume. However, an increased membrane surface area faces the higher risk of membrane rupture *in vivo*, which can cause device failure leading to severe hypoglycemia and even host death. To solve this problem, we designed PDMS grid sheet-covered microdevices with glucose-responsive bioinorganic membranes crosslinked to the PDMS grid, which is adhered to a PDMS reservoir. We chose to use PDMS to form the microdevice structures because of its ease of microfabrication, relatively

accepted biocompatibility for implantable devices particularly for animal studies, its resealing property which is important for drug refilling, and mechanical strength.³⁶ Compared with the soft bioinorganic membranes with a Young's modulus value of approximately 10 kPa,¹² PDMS has a 25 to 50-fold higher Young's modulus value, which is critical for maintaining membrane constitution.^{39,40} These new integrated microdevices increase net insulin permeation and minimize device numbers required for implantation. The integrated PDMS grid also reinforces the albumin-based glucose-responsive permeable membrane, maintaining membrane integrity, with a larger, more efficient area for insulin permeation.

Following *in vitro* testing of the glucose-responsive insulin release from the grid sheet and the microdevices, we conducted *in vivo* testing of the capability of the microdevices to control hyperglycemia in STZ rats. This Type 1 diabetic rat model is an important vehicle for the *in vivo* analysis of prototype insulin microdevices. Utilizing both glucose and insulin assays can quickly provide the information needed to discern the efficacy of microdevices *in vivo*, which cannot ethically be performed in humans. Our microdevices reported in this paper were developed for the diabetic rat model as a proof-of-concept glucose-responsive insulin-delivery system. Achieving glucose-responsive delivery of insulin in a fashion that mimics the way of normal body controlling glycemic profile is the crux of the implantable microdevice system. Furthermore, our implantable insulin-delivery microdevices allow for maintenance of blood glucose under true, untethered *in vivo* conditions, avoiding cannulated attachment and wiring seen with alternate intravenous systems.

Methods

Materials

All materials were analytical grade and used without further purification unless noted. Bovine serum albumin (99%), catalase (solution 13 mg ml⁻¹), 3-aminopropyltrimethoxysilane (97%), glutaraldehyde (25%, Grade I), *n*-octyl- β -glucopyranoside and poly(ethylene glycol) methyl ether (M_w 2000) were purchased from Sigma-Aldrich (USA). Glucose oxidase (230 u mg⁻¹) was purchased from Wisent (Canada). HEPPS (4-(2-hydroxyethyl)-1-piperazinepropanesulfonic acid) was purchased from MP Biomedicals (USA). PDMS, 184 silicone elastomer was obtained from Ellsworth Adhesives Canada (Burlington, ON, Canada). PNIPAM-*co*-PMAA nanoparticles (250 \pm 50 nm in pH 7.4 and 160 \pm 35 nm at pH 5.0 PBS) and nano-MnO₂ nanoparticles (80 \pm 30 nm) were prepared as previously described.^{15,16}

Preparation of activated PDMS grid microdevices

To fabricate glucose-responsive membranes, standard soft lithography was first used for forming a PDMS grid sheet. The insulin reservoir compartment was constructed with PDMS due to its mechanical stability, the feasibility of precise patterning using microfabrication, and its short-term biocompatibility. SU-8 pillars were constructed *via* standard photolithography and used as a mold master (see ESI†). PDMS was spin-coated on the SU-8 mold master. The cured PDMS membrane with a thickness of 150 μ m was peeled off from the substrate, producing a PDMS grid sheet. PDMS grid sheets were bonded with the insulin

reservoir *via* a thin layer of pre-cured PDMS as an adhesive layer. PDMS grid microdevices were modified by oxygen plasma treatment to introduce reactive hydroxyls and then soaked in 0.1 M aminopropyl trimethoxysilane solution for 24 h at room temperature to produce primary amine groups, which provide active sites for covalently crosslinking the bioinorganic membrane to the PDMS grid, improving membrane integrity.²²

Preparation of glucose-responsive bioinorganic PDMS grid–gel microdevices

MnO₂ nanoparticles (6 mg) were dispersed in 143 μl of phosphate buffered saline (pH 4) using a UP100H Hielscher ultrasonicator. Albumin (28 mg), glucose oxidase (3 mg) and catalase (0.86 mg) were added to the suspension and dissolved under light agitation in a 37 °C water bath. To the MnO₂–protein mixture, 65 μl of 200 mg ml⁻¹ NIPAM:MAA hydrogel nanoparticle suspension was added in slowly under stirring with a stir bar. To initiate crosslinking, 25% glutaraldehyde solution (15 μl) was introduced and stirred rapidly for 5 s, and then 60 μl of the mixture was pipetted onto an activated grid device surface and spread evenly. Each batch provided enough volume for three grid device surfaces. Grid–gel membrane devices were allowed to crosslink for 10 min, and then placed in PBS pH 7.4 solution at 4 °C for 24 h.

To reduce the hydrophobicity of PDMS and improve insulin compatibility with the device, we introduced activated polyethylene glycol (PEG) on the PDMS surface. After completion of crosslinking, grid–gel devices were soaked in an activated-PEG solution for 24 h at 4 °C to initiate hydrophilic surface modification of the devices. The devices were washed several times in PBS pH 7.4 to remove soluble unreacted activated-PEG and then incubated in fresh PBS pH 7.4 at 4 °C before use.

ESEM analysis of PDMS grid–bioinorganic gel

Environmental scanning electron microscopy (ESEM) imaging was conducted to analyze the morphology and integrity of crosslinked PDMS grid sheets with bioinorganic gels and the surface of the microdevices. ESEM images were taken at ×160 magnification on membrane grid holes. To determine grid–gel membrane integrity after *in vivo* testing, grid–gel microdevice samples were retrieved 0, 5 and 15 days after *in vivo* implantation and incubated in formalin (1% paraformaldehyde, 4% glutaraldehyde) at 4 °C for 24 h to prepare samples and fix residual cellular adhesion. Retrieved PDMS grid–gel bioinorganic membranes were also analyzed to investigate degradation and cell adhesion for biocompatibility analysis at ×200 magnification.

Reservoir insulin formulation and stability analysis

Insulin formulation was prepared in a buffered solution of 3-[4-(2-hydroxyethyl)-1-piperazinyl]propanesulfonic acid (HEPPS) (pH 7.4). To make 2 ml of 25 mg ml⁻¹ insulin reservoir formulation, 50 mg of human recombinant insulin (*M_w* 5808, Wisent) was dissolved in 1.2 ml 0.1 M NaOH solution. Octyl β-D-glucopyranoside (8 mg) and Pluronic F68 (8 mg) were added as surfactant to stabilize insulin and dissolved slowly. Then 0.252 g of HEPPS was added and 800 μl of 0.1 M HCl was added to adjust pH to approximately 7. Insulin solution was prepared one day before injection into microdevices.

Insulin solution (100 μl) was injected into the PDMS reservoir immediately before implantation into rats using a 27 gauge syringe needle. The self-sealing property of PDMS maintains the integrity of the device after injection. Insulin filled devices were kept in sterile saline solution before implantation. After the implantation period, microdevices were removed and insulin was retrieved from microdevice reservoirs.

Retrieved insulin and freshly prepared samples were analyzed by reversed-phase HPLC using a Waters HPLC equipped with a Waters NovaPak C18 column, 3.9 mm × 150 mm (4.0 μm pore size). The column was eluted with two mobile phase solutions in two-gradient modes at a flow rate of 1 ml min⁻¹. Solvent A was water (0.1% trifluoroacetic acid) and solvent B was acetonitrile (0.1% trifluoroacetic acid). The column was initially run in an 85/15 ratio of A to B, with a linear gradient to 35/65 over 10 min, then returned to 85/15 over 10 min. Insulin samples were detected by a UV detector (Waters PDA 2899) at 215 nm.

In vitro testing of insulin release from microdevices

At the start of experiment, devices were incubated in PBS pH 7.4 at 37 °C with 5 mmol L⁻¹ D-glucose (corresponding to normal glucose levels) and increased to 20 mmol L⁻¹ glucose (corresponding to hyperglycemic glucose levels) after 2.5 h, while slowly rotating on a hematological blot mixer. UV measurements of insulin were taken by an Agilent UV Spectrometer at 276 nm every 30 min. Three normal glucose–high glucose cycles were tested, with multiple washing of microdevices in between to remove residual glucose and insulin from prior tests. A calibration curve was determined with serial dilution of human recombinant insulin stock solution.

The *in vitro* insulin release in response to glucose concentration was measured at 20 mmol L⁻¹ glucose and 5 mmol L⁻¹ glucose in the release medium. From the permeation–time profiles, insulin permeability was determined according to: $P = \frac{s \times h}{a \times c}$, where P = permeability (cm² s⁻¹), s = slope of the permeation *vs.* time plot (mg s⁻¹), h = membrane thickness (cm), a = membrane surface area for permeation (cm²), and c = insulin concentration in the device (mg cm⁻³). Permeability ratio was calculated by dividing the permeability at high glucose by the permeability at low glucose (P_{20}/P_5). Three cycles were plotted to examine microdevice repeatability.

In vivo testing with microdevice-implanted STZ-diabetic rats

All animal experiments were performed in compliance with the relevant laws and institutional guidelines provided by the Division of Comparative Medicine at the University of Toronto (Protocol #: 20009218). Male Sprague-Dawley rats were injected with 65 mg ml⁻¹ streptozotocin (STZ) to induce diabetes 3 days before implantation. STZ destroys pancreatic beta cells, thus removing endogenous insulin production and glycemic control, leading to hyperglycemia. The rats were kept under 12/12 reverse light cycle. Blood glucose was taken before STZ-injection and after to ensure beta cell deficiency. All rats were implanted with a single microdevice in two groups: one group was implanted with a microdevice filled with 25 mg ml⁻¹ insulin formulation and the other group was implanted with a sham microdevice filled with saline as control. Surgery was performed on the abdominal wall of

the rats, and the microdevice was implanted intraperitoneally. Blood glucose was measured on day 0, 1 and 2 and then measured three times a day with a LifeScan OneTouch meter. Blood samples from the tail vein were also taken for insulin and C-peptide measurements by radioimmunoassay which was performed with commercial kits (Linco).

***In vivo* glucose challenge testing with microdevice-implanted STZ-diabetic rats**

In the glucose challenge tests, STZ-diabetic rats treated with insulin microdevices were given a 1 g kg^{-1} injection of glucose *via* a previously cannulated jugular vein to induce hyperglycemia, while blood for glucose, C-peptide and insulin measurements were taken as described before *via* a previously cannulated carotid artery.

Results and discussion

Microdevice working mechanism

As shown in Fig. 1a and 1b, a PDMS drug reservoir and a layer of PDMS grid provide physical support for the bioinorganic composite membrane. In the composite membrane, the enzymes GOx and CAT are directly crosslinked with the albumin macromolecules, as well as suspended nano-MnO₂ particles, forming the base membrane. The hydrogel nanoparticles embedded in the base membrane detect and respond to local pH changes caused by gluconic acid produced from the oxidation of environmental glucose by GOx, acting as intelligent 'nano-valves'.

The MnO₂ nanoparticles and catalase act as catalysts to remove harmful hydrogen peroxide produced by the glucose oxidase reaction and recover consumed oxygen. Volumetric swelling and shrinking of the hydrogel nanoparticles in response to the fluctuation of glucose levels control the porosity of the membrane, resulting in regulated insulin release from the microdevice reservoir, powered by a concentration gradient (Fig. 1c).

With our microdevice system, intraperitoneal implantation allows for rapid response to glucose and delivery of insulin. Fabrication of the devices requires careful integration of PDMS grid to PDMS reservoir, and bioinorganic gel to PDMS grid. Compared with tube-shaped devices developed by Gordijo *et al.*,^{21,22} improved device integrity is achieved in the present microdevices. The reservoir volume of the present microdevices is twice as large as the previous tube-shaped devices ($100 \mu\text{l}$ vs. $50 \mu\text{l}$). Upon incubation in buffer on a rotating mixer for 24 h, none of the fully prepared microdevices showed any signs of rupture or damage that could cause dose dumping *in vivo*.

***In vitro* glucose-responsive insulin release from microdevices**

Using a three-cycle testing protocol, amount of insulin permeated *vs.* time was measured using a clinically relevant glucose concentration change in the buffer solution (5 to 20 mmol L^{-1}). As seen in Fig. 2a, the slope of the curves (rate of insulin release) increased significantly at 2.5 h when glucose concentration was increased from 5 mmol L^{-1} to 20 mmol L^{-1} . All three cycles had a permeability ratio above 2 ($P_{20}/P_5 > 2$) (Fig. 2b and Table 1)

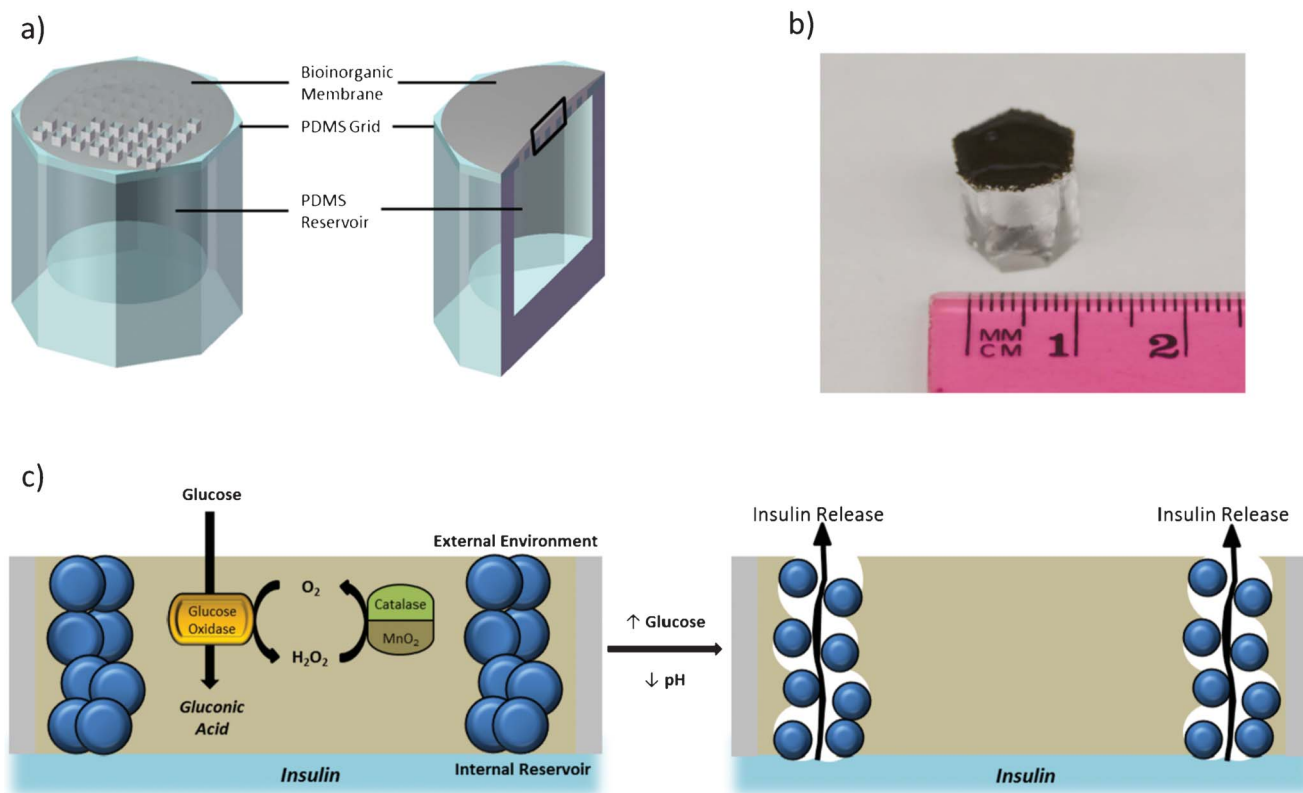


Fig. 1 (a) Schematic of the PDMS grid–gel microdevice with integrated bioinorganic membrane (with inset for (c)). (b) Size comparison of completed PDMS grid–bioinorganic gel membrane microdevices. (c) Cross-sectional diagram showing triggered insulin release in a glucose-rich environment to form open 'nano-pores'.

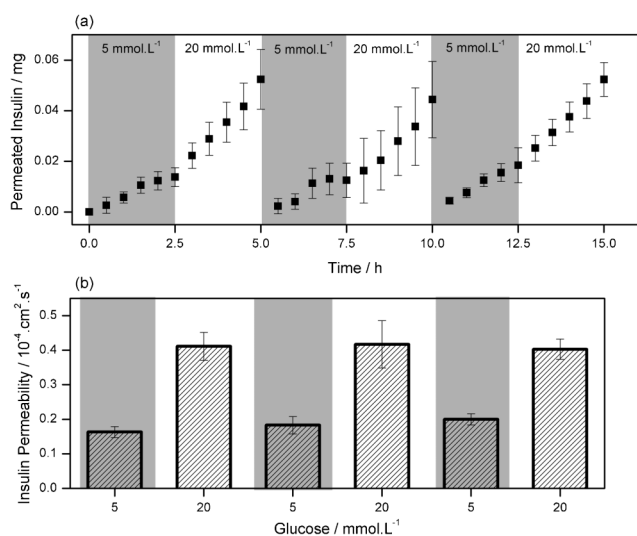


Fig. 2 (a) Three-cycle testing of *in vitro* insulin permeability testing for PDMS grid-gel glucose-responsive microdevices over 5 mmol L⁻¹ (shaded area) and 20 mmol L⁻¹ (open area). Error bars represent standard deviation ($n = 5$). (b) Three-cycle *in vitro* insulin permeability of PDMS grid-gel microdevices. Error bars represent standard deviation ($n = 5$).

Table 1 Three-cycle *in vitro* insulin permeability data for glucose-responsive microdevices

Cycle	P_{20}	P_5	P_{20}/P_5
1	$1.15 \times 10^{-4} \text{ cm}^2 \text{ s}^{-1}$	$4.56 \times 10^{-5} \text{ cm}^2 \text{ s}^{-1}$	2.53
2	$1.17 \times 10^{-4} \text{ cm}^2 \text{ s}^{-1}$	$5.12 \times 10^{-5} \text{ cm}^2 \text{ s}^{-1}$	2.28
3	$1.13 \times 10^{-4} \text{ cm}^2 \text{ s}^{-1}$	$5.60 \times 10^{-5} \text{ cm}^2 \text{ s}^{-1}$	2.01

showing consistent response to glucose levels over multiple cycles. This cyclic response is important for *in vivo* applications under the diabetic condition, as meals can cause large shifts in glucose levels, to which the microdevice has shown a rapid, repeatable response. The amount of insulin released over 4 h was determined to be $49.7 \pm 11.1 \mu\text{g}$, which is clinically relevant as it equates to roughly 5 units per day, within the tolerance range for *in vivo* testing on rats. Based on this finding, only one PDMS grid-gel microdevice per rat was necessary for controlling hyperglycemia, compared with our previous studies that required the implantation of five tube-shaped devices to achieve efficacy.^{21,22}

Morphology and integrity of PDMS grid-gel membrane

As seen in Fig. 3a, the bioinorganic membrane evenly covered the grid holes. Examination of membrane surface showed no gaps in the grid-gel membrane, indicating complete crosslinking of bioinorganic gel membrane to surface-modified PDMS grid. This confirms that the grid-gel membrane interface between the reservoir and the external environment was fully sealed, avoiding issues such as dose dumping. This integrated grid-gel membrane serves as a scaffold for the PDMS reservoir, providing the membrane with strong physical support. Also, this allows for a surface area approximately 4 times larger than previous tube-shaped devices (8 mm^2 vs. 2 mm^2), allowing a higher rate of insulin delivery per device. During incubation in PBS pH 7.4,

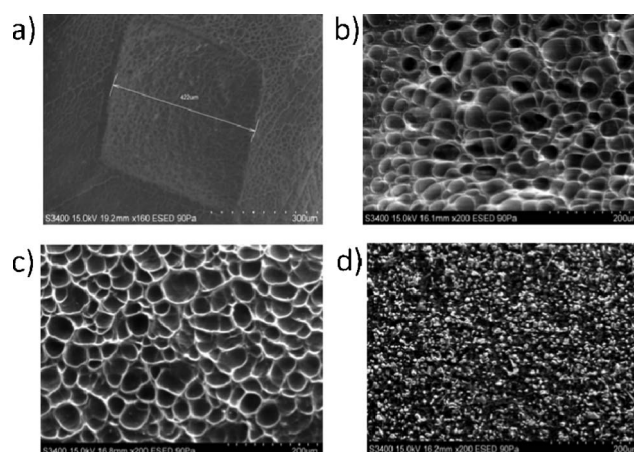


Fig. 3 (a) ESEM image of PDMS grid hole crosslinked with bioinorganic membrane (magnification $\times 160$). Grid holes were on average $420 \mu\text{m}$ wide. ESEM analysis of bioinorganic membrane surface after *in vivo* testing. Comparison of control (day 0) (b), implantation with insulin (day 5) (c) and implantation with saline (day 5) (d) (magnification $\times 200$).

none of the grid holes showed gel membrane damage after agitation in a scintillation vial for 24 h on a rotating stirrer.

Membrane samples were taken from grid-gel microdevices retrieved at the end of experiments and treated with formalin. Comparing the ESEM image of the control bioinorganic microdevice surface (Fig. 3b) with the insulin-loaded bioinorganic microdevice surface (Fig. 3c) after 5 days, there was little change in structure and morphology. Little cellular adhesion and accumulation were seen on the implanted insulin-filled device. However, on the membrane of the microdevice loaded with saline after 5 day implantation, there was heavy buildup of cells, likely resulting from immune response, and a completely different morphology was observed (Fig. 3d). The porous structure of the membrane seemed to have become collapsed or covered with cells. The presence of insulin release from the microdevices appears to exert a positive effect on the biocompatibility of the bioinorganic membrane compared with saline-filled microdevices, although this must be confirmed with further study.

Implanted microdevice controlled hyperglycemia and provided sustained release of insulin

Fig. 4a shows that implanted insulin delivery microdevices can maintain glucose levels in diabetic rats at normoglycemia for at least 7 days, while in the control rats with sham devices, glucose concentrations reached above 20 mmol L^{-1} . In the insulin microdevice-treated group, the blood glucose concentration dropped dramatically after implantation. The blood glucose levels in the microdevice-treated group gradually increased after day 10, possibly due to the depletion of reservoir insulin or insulin inactivation over time. The insulin microdevice-treated rats were healthy with no mortality seen in any of the subjects.

Insulin profiles for the treated group and control group are presented in Fig. 4b. The insulin levels in the control group were very low as expected, much lower than normal physiological levels due to destruction of the pancreatic beta cells. Insulin microdevice-treated rats showed a rapid increase in insulin levels after implantation, with the insulin relatively stable over ten

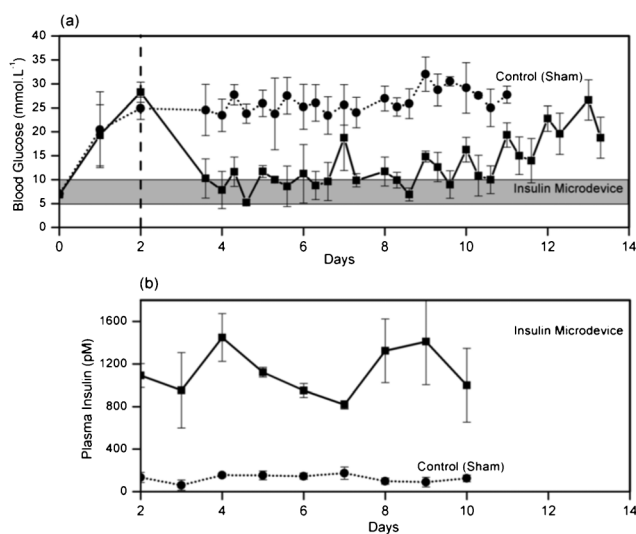


Fig. 4 (a) Long-term plasma blood glucose measurements in STZ-diabetic rats. Shaded area indicates normoglycemic range. Implantation of microdevices occurred at day 2. Error bars represent standard error ($n = 5$). (b) Long-term plasma insulin measurements in STZ-diabetic rats. Implantation of microdevices occurred at day 2. Error bars represent standard error ($n = 5$).

days. The plasma insulin levels in the microdevice implanted rats were high; however, the rats did not show associated hypoglycemic conditions, which suggests a possibility of compensation for reduced insulin bioactivity or insulin insensitivity (Fig. 4b).

Implanted insulin microdevice response to glucose challenge

To examine if the glycemia-control effect of the insulin microdevices was due to sustained insulin release or glucose-responsive insulin release, a short-term glucose challenge test was conducted on diabetic rats with implanted insulin microdevices. Fig. 5a shows that after the injection of a 1 g kg^{-1} bolus of glucose, the blood glucose peaks at 2 min followed by a drastic decrease. Over the next 30 min, blood glucose returned to normal baseline levels (Fig. 5a). Fig. 5b shows that insulin release was regulated by glucose concentration. After glucose challenge, plasma insulin concentrations increased immediately and significantly by 300 pM at 10 min. Once blood glucose returned to normal, insulin concentrations leveled off at 30 min and onwards (Fig. 5b).

Absolute C-peptide, an indicator of endogenous insulin production, was assayed to investigate if the insulin was from the microdevices or from the endogenous source. Fig. 5c shows no change in C-peptide concentration with glucose level, indicating that the rise in insulin level was not from residual β -cell activity. These results demonstrate the capability of the microdevices to release insulin in response to glucose levels. Furthermore, these results agree with the previous findings with tube-shaped devices,^{21,22} demonstrating that the implantable microdevice can provide glucose-responsive insulin release on demand.

Stability of insulin retrieved from *ex vivo* microdevices

Remaining insulin retrieved from the microdevice reservoirs after *in vivo* implantation was examined by RP-HPLC for studying structural integrity and formulation stability. The chromatograms of insulin retrieved one day after the 14 day implantation

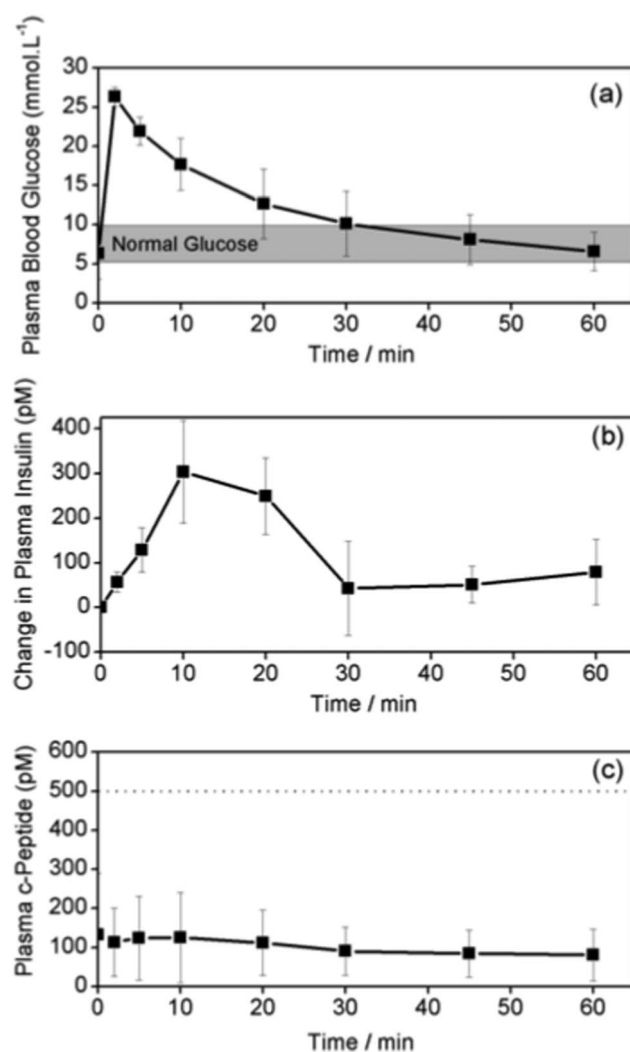


Fig. 5 (a) Plasma blood glucose in STZ-diabetic rats with implanted microdevices after glucose challenge at $t = 0$. Error bars represent standard deviation ($n = 3$). Normal glucose range indicated by shaded area. (b) Change in plasma insulin measurements in STZ-diabetic rats with implanted microdevices after glucose challenge at $t = 0$. Error bars represent standard deviation ($n = 3$). (c) Plasma C-peptide measurements in STZ-diabetic rats with implanted microdevices after glucose challenge at $t = 0$. Error bars represent standard deviation ($n = 3$). Dotted lines represent normal physiological levels of C-peptide.

was compared with fresh human recombinant insulin and intraperitoneal (IP) fluid (Fig. S2 in the ESI[†]). The insulin peak at 8.7 min elution time was still present in the retrieved samples, suggesting insulin did not degrade into denatured products, because aggregated insulin samples usually produce a much wider, erratic peak at a broad range of retention times, as reported in the literature.^{30,37,38} However, a second peak was found in the retrieved insulin samples, which seems to match with the peak from the IP fluid samples. It is possible that some protein in the IP fluid infiltrated the membrane and mixed with the insulin in the microdevice reservoir. The *in vivo* data (Fig. 4b) showed much higher insulin levels than normal physiological levels in normal rats, suggesting that insulin bioactivity was possibly compromised in part. Although the high insulin levels did not adversely affect the rat survival rates or glucose profiles,

this phenomenon needs to be better understood for improving insulin formulations in our future studies.

The goal for implantable microdevices is to provide a self-regulated approach to insulin therapy. The current proof-of-concept system was designed to allow potential future refilling for long-term efficacy, utilizing the resealing property of the PDMS material. The vicinity of the sensor (glucose oxidase) to the release mechanism (hydrogel nanoparticles) is necessary for the rapid response and insulin release for our microdevice. As well, a backup external glucose sensor can be utilized with this system for patients to monitor blood glucose levels.

One concern for this microdevice to translate into human testing versus a rat model is the variability of insulin dosing. The Sprague-Dawley rat model is a controlled group of identical species and similar body weights. Human dosing schedule is based upon insulin sensitivity, glucose metabolism and weight (measured *via* unit kg⁻¹), and must be finely tuned before a safe and efficacious implantable microdevice can be achieved. Furthermore, insulin dosing must be controlled with respect to carbohydrate levels in meals. The results reported in this paper demonstrate our recent progress in the controlled STZ-diabetic rat model. Devices will undergo critical optimization before clinical trials can be considered.

Conclusion

This paper presented new PDMS grid-gel integrated glucose-responsive microdevices and *in vitro* and *in vivo* testing results. Glucose-responsiveness was realized through a glucose-triggered acidic byproduct causing a reversible volumetric shrink/swell dynamic of embedded nanohydrogels and alteration of membrane permeability, without the use of electronic input. Device performance was maintained over multiple cycles *in vitro*, with insulin released at clinically relevant glucose levels. *In vivo* efficacy of the microdevices for hyperglycemia control was maintained for a period of 7 days. Under glucose challenge, these microdevices responded with an acute increase in insulin delivery within minutes, attenuating blood glucose levels. Like all implantable devices, avoiding complications of surgical administration is not possible. However, these proof-of-concept microdevices demonstrated their feasibility for use in studying diabetes in animal models.

Acknowledgements

The authors acknowledge the Natural Sciences and Engineering Research Council of Canada (NSERC) and Canadian Institutes of Health Research (CIHR) for financial support *via* a Collaborative Health Research Projects (CHRP) grant; Banting and Best Diabetes Center for a Postdoctoral Fellowship to C. Gordijo; and Jason Li for his assistance in drawing the microdevice diagram.

References

- J. E. Shaw, R. A. Sicree and P. Z. Zimmet, *Diabetes Res. Clin. Pract.*, 2010, **87**, 4–14.
- D. U. Silverthorn, *Human Physiology: An Integrated Approach*, 4th edition, Pearson Education, 2007, **ch. 6**.
- J. C. Pickup, Z. L. Zhi, F. Khan, T. Saxl and D. J. S. Birch, *Diabetes Metab. Res. Rev.*, 2008, **24**, 604.
- J. Weng, Y. Li, W. Xu, L. Shi, Q. Zhang, D. Zhu, Y. Hu, Z. Zhou, X. Yan, H. Tian, X. Ran, Z. Luo, J. Xian, L. Yan, F. Li, L. Zeng, Y. Chen, L. Yang, S. Yan, J. Liu, M. Li, Z. Fu and H. Cheng, *Lancet*, 2008, **371**, 1753–1760.
- M. Franciosi, A. Maione, B. Pomili, R. Amoretti, E. Busetto, F. Capani, D. Bruttomesso, P. Di Bartolo, A. Girelli, F. Leonetti, L. Morviducci, P. Ponzi, E. Vitacolonna and A. Nicolucci, *Nutr., Metab. Cardiovasc. Dis.*, 2010, **20**, 7–14.
- H. Zisser, L. Robinson, W. Bevier, E. Dassau, C. Ellingsen, F. J. Doyle and L. Jovanovic, *Diabetes Technol. Ther.*, 2008, **10**, 441–444.
- I. B. Hirsch, J. Abelseh, B. W. Bode, J. S. Fischer, F. R. Kaufman, J. Mastrototaro, C. G. Parkin, H. A. Wolpert and B. A. Buckingham, *Diabetes Technol. Ther.*, 2008, **10**, 377–383.
- T. Aye, J. Block and B. Buckingham, *Endocrinol. Metab. Clin. North Am.*, 2010, **39**, 609–624.
- J. J. Mastrototaro, K. W. Cooper, G. Soundararajan, J. B. Sanders and R. V. Shah, *Adv. Ther.*, 2006, **23**, 725–732.
- M. Halvorson, S. Carpenter, K. Kaiserman and F. R. Kaufman, *J. Pediatr.*, 2007, **150**, 103–105.
- R. M. Bergenstal, W. V. Tamborlane, A. Ahmann, J. B. Buse, G. Dailey, S. N. Davis, C. Joyce, T. Peoples, B. A. Perkins, J. B. Welsh, S. M. Willi and M. A. Wood, *N. Engl. J. Med.*, 2010, **363**, 311–320.
- J. Kost and R. Langer, *Adv. Drug Delivery Rev.*, 2001, **46**, 125.
- T. Traitel, R. Goldbart and J. Kost, *J. Biomater. Sci., Polym. Ed.*, 2008, **19**, 755.
- K. Zhang and X. Y. Wu, *J. Controlled Release*, 2002, **80**, 169.
- T. G. Farmer Jr., T. F. Edgar and N. A. Peppas, *J. Pharm. Pharmacol.*, 2008, **60**, 1–13.
- C. Malitesta, F. Palmisano, L. Torsi and P. G. Zambonin, *Anal. Chem.*, 1990, **62**, 2735–2740.
- Y. Sun, X. Zhang, C. Sun, B. Wang and J. Shen, *Macromol. Chem. Phys.*, 1996, **197**, 147–153.
- F. Cui, C. He, M. He, C. Tang, L. Yin, F. Qian and C. Yin, *J. Biomed. Mater. Res.*, 2009, **89**, 1063–1071.
- H. Iwata and T. Matsuda, *J. Membr. Sci.*, 1988, **38**, 185–199.
- P. Kurian, B. Kasibhatla, J. Daum, C. A. Burns, M. Moosa, K. S. Rosenthal and J. P. Kennedy, *Biomaterials*, 2003, **24**, 3493–3503.
- C. R. Gordijo, A. J. Shuhendler and X. Y. Wu, *Adv. Funct. Mater.*, 2010, **20**, 1404–1412.
- C. R. Gordijo, K. Koulajian, A. J. Shuhendler, L. D. Bonifacio, H. Y. Huang, S. Chiang, G. A. Ozin, A. Giacca and X. Y. Wu, *Adv. Funct. Mater.*, 2011, **21**, 73–82.
- W. Wu, N. Mitra, E. C. Y. Yan and S. Zhou, *ACS Nano*, 2010, **4**, 4831–4839.
- J. F. Mano, *Adv. Eng. Mater.*, 2008, **10**, 515–527.
- K. Podual, F. J. Doyle III and N. A. Peppas, *J. Controlled Release*, 2000, **67**, 9–17.
- R. V. Ulijina, N. Bibia, V. Jayawarnaa, P. D. Thornton, S. J. Todd, R. J. Marta, A. M. Smith and J. E. Gough, *Bioresponsive Hydrogels*, 2007, **10**, 40–48.
- Y. Qiu and K. Park, *Adv. Drug Delivery Rev.*, 2001, **53**, 321–339.
- N. Kashyap, B. Viswanad, G. Sharma, V. Bhardwaj, P. Ramarao and M. N. V. Ravi Kumar, *Biomaterials*, 2007, **28**, 2051–2060.
- A. Napoli, M. J. Boerakker, N. Tirelli, J. Roeland, M. Nolte, N. A. J. M. Sommerdijk and J. A. Hubbell, *Langmuir*, 2004, **20**, 3487–3491.
- J. Brange, *Stability of insulin: studies on the physical and chemical stability of insulin in pharmaceutical formulation*, Springer, 1994.
- F. F. Yam and X. Y. Wu, *Polymer Preprint*, 1999, **40**, 312–313.
- F. Yam, X. Y. Wu and Q. Zhang, *Controlled Drug Delivery: Designing Technology for the Future*, ed. K. Park, ACS, Washington, DC, pp. 263–272.
- X. Y. Wu and P. I. Lee, Synthesis and characterization of thermal and pH-sensitive nanospheres., *Pharm. Res.*, 1993, **10**, 1544–1547.
- K. Zhang, H. Huang, G. Yang, J. Shaw, C. Yip and X. Y. Wu, *Biomacromolecules*, 2004, **5**, 1248–1255.
- K. Zhang and X. Y. Wu, *Biomaterials*, 2004, **25**, 5281–5291.
- J. Chen, M. Chu, K. Koulajian, X. Y. Wu, A. Giacca and Y. Sun, *Biomed. Microdevices*, 2009, **11**, 1251–1257.
- K. Zhang, C. Quan, H. Huang, N. Taulier and X. Y. Wu, *J. Pharm. Pharmacol.*, 2004, **56**, 611–620.
- A. Taluja and Y. H. Bae, *Mol. Pharmaceutics*, 2007, **4**, 561–570.
- J. C. Lötters, W. Olthuis, P. H. Veltink and P. Bergveld, *J. Micromech. Microeng.*, 1997, **7**, 145–147.
- X. Y. Liu, R. Fernandes, A. Jurisicova, R. Casper and Y. Sun, *Lab Chip*, 2010, **10**, 2154–2161.